DOI: 10.1021/ic101340a

Inorganic Chemistry
Article

Indium Flux-Growth of Eu_2AuGe_3: A New Germanide with an AlB_2 Superstructure

C. Peter Sebastian,[†] Christos D. Malliakas,[†] Maria Chondroudi,[‡] Inga Schellenberg,[§] Sudhindra Rayaprol,[∥] Rolf-Dieter Hoffmann,[§] Rainer Pöttgen,[*,§] and Mercouri G. Kanatzidis[*,†,‡]

[†]*Department of Chemistry, Northwestern University, 2145 N. Sheridan Road, Evanston, Illinois 60208-3113,* [‡]*Materials Science Division, Argonne National Laboratory, Argonne, Illinois 60439,* [§]*Institut für Anorganische und Analytische Chemie and NRW Graduate School of Chemistry, Westfälische Wilhelms-Universität Münster, Corrensstrasse 30, 48149 Münster, Germany, and* [∥]*UGC-DAE Consortium for Scientific Research, Mumbai Centre, BARC, R-5 Shed, Trombay, Mumbai-400085, India*

Received July 5, 2010

The germanide Eu_2AuGe_3 was obtained as large single crystals in high yield from a reaction of the elements in liquid indium. At room temperature Eu_2AuGe_3 crystallizes with the Ca_2AgSi_3 type, space group *Fmmm*, an ordered variant of the AlB_2 type: a = 857.7(4), b = 1485.5(10), c = 900.2(4) pm. The gold and germanium atoms build up slightly distorted graphite-like layers which consist of Ge_6 and Au_2Ge_4 hexagons, leading to two different hexagonal-prismatic coordination environments for the europium atoms. Magnetic susceptibility data showed Curie−Weiss law behavior above 50 K and antiferromagnetic ordering at 11 K. The experimentally measured magnetic moment indicates divalent europium. The compound exhibits a distinct magnetic anisotropy based on single crystal measurements and at 5 K it shows a metamagnetic transition at ∼10 kOe. Electrical conductivity measurements show metallic behavior. The structural transition at 130 K observed in the single crystal data was very well supported by the conductivity measurements. ^{151}Eu Mössbauer spectroscopic data show an isomer shift of −11.24 mm/s at 77 K, supporting the divalent character of europium. In the magnetically ordered regime one observes superposition of two signals with hyperfine fields of 26.0 (89%) and 3.5 (11%) T, respectively, indicating differently ordered domains.

Introduction

Rare earth (*RE*) based intermetallic compounds have remarkably diverse crystal structures as well as magnetic and electronic properties.[1−3] Among them europium is special because it can adopt different oxidation states, (i) divalent magnetic (Eu^{2+}),[4−8] (ii) trivalent nonmagnetic (Eu^{3+})[9] and/or (iii) even the mixed-valent state.[6,10−14] Generally, such intermetallic compounds are prepared by arc-melting techniques, but because europium is volatile at high temperatures (boiling point 1597 °C) it is difficult to use this technique for their synthesis. The metal flux technique is an excellent tool for exploring novel intermetallic compounds.[15−25]

*To whom correspondence should be addressed. E-mail: pottgen@uni-muenster.de (R.P.), m-kanatzidis@northwestern.edu (M.G.K.).

(1) Crystal Structures and Crystal Chemistry of Ternary Rare Earth Transition Metal Borides, Silicides and Homologues. In *Handbook on the Physics and Chemistry of Rare Earths*; Parthé, E., Chabot, B., Eds.; Elsevier: New York, 1984; Vol. *48*.
(2) *Handbook of Crystal Structures and Magnetic Properties of Rare Earth Intermetallics*.; Szytula, A., Leciejewicz, J., Eds.; CRC Press: Boca Raton: FL, 1994.
(3) *Pearson's Handbook of Crystallographic Data for Intermetallic Compounds*, 2nd ed.; Villars, P., Calvert, L. D., Eds.; American Society for Metals: Materials Park, OH, 1997.
(4) Cho, E. J.; Oh, S. J.; Suga, S.; Suzuki, T.; Kasuya, T. *J. Electron Spectrosc. Relat. Phenom.* **1996**, *77*, 173–181.
(5) Ferreira, L. M.; Bittar, E. M.; Pires, M. A.; Urbano, R. R.; Aguero, O.; Torriani, I.; Rettori, C.; Pagliuso, P. G.; Malachias, A.; Granado, E.; Caytuero, A.; Baggio-Saitovich, E. *Phys. B* (*Amsterdam, Neth.*) **2006**, *384*, 332–335.
(6) Mayer, I.; Felner, I. *J. Phys. Chem. Solids* **1977**, *38*, 1031–1034.
(7) Pöttgen, R.; Hoffmann, R.-D.; Möller, M. H.; Kotzyba, G.; Künnen, B.; Rosenhahn, C.; Mosel, B. D. *J. Solid State Chem.* **1999**, *145*, 174–181.
(8) Prabhawalkar, V.; Padalia, B. D. *Phys. Status Solidi B* **1984**, *121*, K65–K68.
(9) De Vries, J. W. C.; Thiel, R. C.; Buschow, K. H. J. *Phys. B & C* (*Amsterdam, Neth.*) **1984**, *124*, 291–298.
(10) Felner, I.; Nowik, I. *Solid State Commun.* **1978**, *28*, 67–70.
(11) Felser, C. *J. Alloys Compd.* **1997**, *262*, 87–91.
(12) Ksenofontov, V.; Kandpal, H. C.; Ensling, J.; Waldeck, M.; Johrendt, D.; Mewis, A.; Gütlich, P. G.; Felser, C. *Europhys. Lett.* **2006**, *74*, 672–678.
(13) Lux, C.; Mewis, A.; Lossau, N.; Michels, G.; Schlabitz, W. *Z. Anorg. Allg. Chem.* **1991**, *593*, 169–180.
(14) Michels, G.; Junk, S.; Lossau, N.; Schlabitz, W.; Wohlleben, D.; Johrendt, D.; Mewis, A.; Sauer, C.; Woike, T. *Z. Phys. B* **1992**, *86*, 53–58.
(15) Chen, X. Z.; Small, P.; Sportouch, S.; Zhuravleva, M.; Brazis, P.; Kannewurf, C. R.; Kanatzidis, M. G. *Chem. Mater.* **2000**, *12*, 2520–2522.
(16) Chondroudi, M.; Balasubramanian, M.; Welp, U.; Kwok, W. K.; Kanatzidis, M. G. *Chem. Mater.* **2007**, *19*, 4769–4775.
(17) Gray, D. L.; Francisco, M. C.; Kanatzidis, M. G. *Inorg. Chem.* **2008**, *47*, 7243–7248.
(18) Kanatzidis, M. G.; Pöttgen, R.; Jeitschko, W. *Angew. Chem., Int. Ed.* **2005**, *44*, 6996–7023.
(19) Salvador, J. R.; Gour, J. R.; Bilc, D.; Mahanti, S. D.; Kanatzidis, M. G. *Inorg. Chem.* **2004**, *43*, 1403–1410.
(20) Salvador, J. R.; Kanatzidis, M. G. *Inorg. Chem.* **2006**, *45*, 7091–7099.
(21) Zhuravleva, M. A.; Chen, X. Z.; Wang, X. P.; Schultz, A. J.; Ireland, J.; Kannewurf, C. K.; Kanatzidis, M. G. *Chem. Mater.* **2002**, *14*, 3066–3081.

Published on Web 09/13/2010

In comparison to many other metal fluxes, indium is remarkably good in dissolving Si, Ge, rare earth elements, and transition metals and can yield well shaped crystals of new materials. One example is the kinetic and thermodynamic α and β forms of $RENiGe_2$[19] with $YIrGe_2$ and $CeNiSi_2$ type structure, respectively, obtained from reactions run in liquid indium as flux medium. Several compounds such as $CeTIn_5$ (T = Rh, Ir),[26,27] Ce_2TIn_8 (T = Rh, Ir),[28] $CeNiIn_2$,[29] $Tb_6Pt_{12}In_{23}$,[30] and $Dy_2Pt_7In_{16}$[30] were grown as large single crystals in indium fluxes by recrystallizing arc melted samples. The synthesis of $YbTIn_5$ (T = Co, Rh, Ir),[31,32] used an excess of indium already in the starting composition. Generally, liquid indium has been little exploited as a synthetic flux compared to Al[33−41] and Ga;[15,22,23,38−40,42−46] however, interest in this powerful flux has been increasing.[16,20,47−50]

During our systematic phase analytical investigations using metal fluxes, we have now investigated the Eu−Au−Ge system using liquid indium as flux medium, to overcome the synthetic difficulties of the arc-melting technique. So far only the AlB_2 type solid solution $EuAu_{0.54}Ge_{1.46}$ ($P6/mmm$),[51] the equiatomic germanide EuAuGe,[52,53] an ordered superstructure of the KHg_2 type (space group $Imm2$), and $ThCr_2Si_2$ type $EuAu_2Ge_2$[54−56] have been reported. Herein we report the structure and properties of the new germanide Eu_2AuGe_3 grown from the reaction of Eu, Au, and Ge in an indium metal flux. We discovered that Eu_2AuGe_3 undergoes a structural phase transition at 130 K that is accompanied with a change to an orthorhombic space group as well as antiferromagnetic transitions at lower temperatures.

Experimental Section

Reagents. The following reagents were used as purchased without further purification: Eu (metal chunk, 99.9%, Chinese Rare Earth Information Center, Inner Mongolia, China), Au (pieces, 99.9% Alfa Aesar, Ward Hill, MA), Ge (ground from 2−5 mm pieces 99.999% Plasmaterials, Livermore, CA) and In (tear drops 99.99% Cerac, Milwauke, WI).

Synthesis−Method 1. Eu_2AuGe_3 was obtained by combining 3 mmol of europium metal, 2 mmol of gold, 6 mmol of germanium, and 45 mmol of indium in an alumina crucible under an inert nitrogen atmosphere inside a glovebox. The crucible was placed in a 13 mm fused silica tube, which was flame-sealed under vacuum of 10^{-4} Torr, to prevent oxidation during heating. The reactants were then heated to 1000 °C over 10 h, maintained at that temperature for 5 h to allow proper homogenization, followed by cooling to 850 °C in 2 h and held there for 48 h. Finally, the sample was allowed to slowly cool to 50 °C in 48 h. The reaction product was isolated from the excess indium flux by heating at 350 °C and subsequent centrifugation through a coarse frit. Any remaining flux was removed by immersion and sonication in glacial acetic acid for 48 h. The final crystalline product was rinsed with water and dried with acetone. Several crystals of Eu_2AuGe_3, which grow as metallic silvery rods were carefully selected for elemental analysis, structure characterization, and physical property measurements. The other products observed from the synthesis are $EuGe_2$ and AuIn. The light gray rod shaped single crystals of Eu_2AuGe_3 up to 4 mm in length were stable in air, and no decomposition was observed even after several months. Single crystals have metallic luster.

Synthesis−Method 2. Europium, gold, and germanium were mixed in the ideal 2:1:3 atomic ratio and sealed in a tantalum ampule under an argon atmosphere in an arc-melting apparatus. The tantalum ampule was subsequently placed in a water-cooled sample chamber of an induction furnace (EasyHeat induction heating system, Model 7590), first rapidly heated to about 1250 K and kept at that temperature for 10 min. Finally the temperature was lowered to 1000 K and the sample was annealed at that temperature for another 30 min, followed by quenching by switching off the power supply. The brittle product could easily be separated from the tantalum tube. No reaction with the container was observed. The obtained compound is pure up to the level of powder X-ray diffraction.

Elemental Analysis. Quantitative microprobe analyses of the samples were performed with a Hitachi S-3400 scanning electron

(22) Zhuravleva, M. A.; Kanatzidis, M. G. *J. Solid State Chem.* **2003**, *173*, 280–292.
(23) Zhuravleva, M. A.; Pcionek, R. J.; Wang, X. P.; Schultz, A. J.; Kanatzidis, M. G. *Inorg. Chem.* **2003**, *42*, 6412–6424.
(24) Zhuravleva, M. A.; Salvador, J.; Bilc, D.; Mahanti, S. D.; Ireland, J.; Kannewurf, C. R.; Kanatzidis, M. G. *Chem.—Eur. J.* **2004**, *10*, 3197–3208.
(25) Zhuravleva, M. A.; Wang, X. P.; Schultz, A. J.; Bakas, T.; Kanatzidis, M. G. *Inorg. Chem.* **2002**, *41*, 6056–6061.
(26) Hegger, H.; Petrovic, C.; Moshopoulou, E. G.; Hundley, M. F.; Sarrao, J. L.; Fisk, Z.; Thompson, J. D. *Phys. Rev. Lett.* **2000**, *84*, 4986–4989.
(27) Moshopoulou, E. G.; Fisk, Z.; Sarrao, J. L.; Thompson, J. D. *J. Solid State Chem.* **2001**, *158*, 25–33.
(28) Macaluso, R. T.; Sarrao, J. L.; Moreno, N. O.; Pagliuso, P. G.; Thompson, J. D.; Fronczek, F. R.; Hundley, M. F.; Malinowski, A.; Chan, J. Y. *Chem. Mater.* **2003**, *15*, 1394–1398.
(29) Zaremba, V. I.; Kalychak, Y. M.; Tyvanchuk, Y. B.; Hoffmann, R.-D.; Möller, M. H.; Pöttgen, R. *Z. Naturforsch.* **2002**, *57b*, 791–797.
(30) Zaremba, V. I.; Kalychak, Y. M.; Dubenskiy, V. P.; Hoffmann, R.-D.; Rodewald, U. C.; Pöttgen, R. *J. Solid State Chem.* **2002**, *169*, 118–124.
(31) Zaremba, V. I.; Rodewald, U. C.; Hoffmann, R.-D.; Kalychak, Y. M.; Pöttgen, R. *Z. Anorg. Allg. Chem.* **2003**, *629*, 1157–1161.
(32) Zaremba, V. I.; Rodewald, U. C.; Pöttgen, R. *Z. Naturforsch.* **2003**, *58b*, 805–808.
(33) Chen, X. Z.; Sportouch, S.; Sieve, B.; Brazis, P.; Kannewurf, C. R.; Cowen, J. A.; Patschke, R.; Kanatzidis, M. G. *Chem. Mater.* **1998**, *10*, 3202–3211.
(34) Sieve, B.; Chen, X. Z.; Henning, R.; Brazis, P.; Kannewurf, C. R.; Cowen, J. A.; Schultz, A. J.; Kanatzidis, M. G. *J. Am. Chem. Soc.* **2001**, *123*, 7040–7047.
(35) Sieve, B.; Sportouch, S.; Chen, X. Z.; Cowen, J. A.; Brazis, P.; Kannewurf, C. R.; Papaefthymiou, V.; Kanatzidis, M. G. *Chem. Mater.* **2001**, *13*, 273–283.
(36) Latturner, S. E.; Kanatzidis, M. G. *Inorg. Chem.* **2002**, *41*, 5479–5486.
(37) Latturner, S. E.; Bilc, D.; Mahanti, S. D.; Kanatzidis, M. G. *Chem. Mater.* **2002**, *14*, 1695–1705.
(38) Latturner, S. E.; Bilc, D.; Mahanti, S. D.; Kanatzidis, M. G. *Inorg. Chem.* **2003**, *42*, 7959–7966.
(39) Latturner, S. E.; Kanatzidis, M. G. *Chem. Commun.* **2003**, 2340–2341.
(40) Latturner, S. E.; Bilc, D.; Ireland, J. R.; Kannewurf, C. R.; Mahanti, S. D.; Kanatzidis, M. G. *J. Solid State Chem.* **2003**, *170*, 48–57.
(41) Latturner, S. E.; Kanatzidis, M. G. *Inorg. Chem.* **2008**, *47*, 2089–2097.
(42) Chen, X. Z.; Larson, P.; Sportouch, S.; Brazis, P.; Mahanti, S. D.; Kannewurf, C. R.; Kanatzidis, M. G. *Chem. Mater.* **1999**, *11*, 75–83.
(43) Zhuravleva, M. A.; Kanatzidis, M. G. *Z. Naturforsch.* **2003**, *58b*, 649–657.
(44) Zhuravleva, M. A.; Evain, M.; Petricek, V.; Kanatzidis, M. G. *J. Am. Chem. Soc.* **2007**, *129*, 3082–3083.
(45) Latturner, S. E.; Bryan, J. D.; Blake, N.; Metiu, H.; Stucky, G. D. *Inorg. Chem.* **2002**, *41*, 3956–3961.
(46) Salvador, J. R.; Malliakas, C.; Gour, J. R.; Kanatzidis, M. G. *Chem. Mater.* **2005**, *17*, 1636–1645.
(47) Bailey, M. S.; McGuire, M. A.; DiSalvo, F. J. *J. Solid State Chem.* **2005**, *178*, 3494–3499.
(48) Benbow, E. M.; Latturner, S. E. *J. Solid State Chem.* **2006**, *179*, 3989–3996.
(49) Klünter, W.; Jung, W. *J. Solid State Chem.* **2006**, *179*, 2880–2888.
(50) Zaremba, V. I.; Dubenskiy, V. P.; Rodewald, U. C.; Heying, B.; Pöttgen, R. *J. Solid State Chem.* **2006**, *179*, 891–897.
(51) Pöttgen, R.; Grin, Y. *Z. Kristallogr.* **1997**, No. Suppl. 12, 137.
(52) Pöttgen, R. *J. Mater. Chem.* **1995**, *5*, 505–508.
(53) Müllmann, R.; Mosel, B. D.; Eckert, H.; Pöttgen, R.; Kremer, R. K. *Hyperfine Interact.* **1997**, *108*, 389–400.
(54) Wortmann, G.; Perscheid, B.; Krone, W. *J. Phys. Coll. C8* **1986**, *47*, C8−979–C8−982.
(55) Hesse, H.-J; Wortmann, G. *Hyperfine Interact.* **1994**, *93*, 1499–1504.
(56) Schellenberg, I.; Hermes, W.; Lidin, S.; Pöttgen, R. *Z. Kristallogr.*, submitted for publication.

Table 1. Crystal Data and Structure Refinement for the Room Temperature Structure of Eu_2AuGe_3

refined composition	Eu_2AuGe_3
temperature	295 K
formula mass (g mol^{-1})	718.66
space group	*Fmmm* (No. 69)
formula units/cell, Z	8
unit cell dimensions (pm)	a = 857.7(4)
(Guinier powder data)	b = 1485.5(10)
	c = 900.2(4)
cell volume (nm^3)	V = 1.1470
calculated density (g cm^{-3})	8.32
crystal dimensions (μm)	20 × 40 × 60
range in θ	2−27°
detector distance (mm)	120
exposure time (min)	5
ω-range; $\Delta\omega$	0−180°; 1°
ϕ-positions	76°; 106°; 136°; 166°
integr. param. A, B, EMS	14.0; 2.0; 0.030
transm. ratio (max/min)	0.442/0.116
absorption coeff. (mm^{-1})	62.4
F(000)	2408
range in *hkl*	$-10 \le h \le 10$
	$-18 \le k \le 18$
	$-11 \le l \le 11$
total no. of reflections	2324
independent reflections	361 (R_{int} = 0.0622)
reflections with $I > 2\sigma(I)$	261 (R_σ = 0.0721)
data/parameter	361/23
goodness-of-fit on F^2	0.659
final R indices[a]	R1 = 0.0283
[$I > 2\sigma(I)$]	wR2 = 0.0320
final R indices (all data)[a]	R1 = 0.0421
	wR2 = 0.0345
extinction parameter	0.00085(3)
largest diff. peak/hole	3.26/−3.50 e Å^{-3}

[a] $R = \sum||F_o| - |F_c||/\sum|F_o|$, $wR = \{\sum w(F_o^2 - F_c^2)^2/\sum w(|F_o|^4)\}^{1/2}$ and $w = 1/(\sigma^2(I) + 0.0016I^2)$.

microscope (SEM) equipped with a PGT energy dispersive X-ray analyzer. Data were acquired with an accelerating voltage of 20 kV and a 60 s accumulation time. The energy dispersive spectroscopy (EDS) analysis taken on visibly clean surfaces of the samples gave the atomic composition close to 2:1:3.

X-ray Powder and Single Crystal Data. X-ray powder data were collected on an Inel diffractometer using CuKα_1 radiation and Si as standard. The orthorhombic lattice parameters (Table 1) were refined through a least-squares routine. Proper indexing was ensured through an intensity calculation[57] using the data of the refined subcell structure (vide infra). Small crystal fragments were isolated from crushed larger flux grown crystals and mounted on quartz fibers using bees wax. The crystals were investigated on a Buerger precession camera (white Mo radiation, Fujifilm imaging plate) to check the quality for intensity data collection. The data set was collected at room temperature by use of an IPDS II diffractometer (graphite monochromatized Mo Kα radiation; oscillation mode). A numerical absorption correction was applied to the data set. Details on the crystallographic data are given in Table 1.

Structure Refinement. The room temperature data set of Eu_2AuGe_3 was compatible with space group *Fmmm*, in agreement with earlier work on Ca_2AgSi_3.[58] The atomic parameters of the calcium compound were then taken as starting values, and the Eu_2AuGe_3 structure was refined with SHELXL−97 (full-matrix least-squares on F^2)[59] with anisotropic atomic displacement parameters for all atoms. Refinement of the occupancy parameters showed full occupancy within two standard deviations. In contrast to Ca_2AgSi_3,[58] where all sites showed almost isotropic displacements, the gold and especially the two germanium atoms in Eu_2AuGe_3 exhibit larger U_{33} values. Careful investigation of the reciprocal space of the room temperature data set (calculation of the 3D file with the BuildSpace routine of the Stoe IPDS X-Area package) gave no hint for superstructure reflections or diffuse scattering.

The final difference electron-density synthesis was flat. The results of the structure refinement are summarized in Table 1. The atomic coordinates and the interatomic distances are listed in Tables 2 and 3. Further information on the structure refinement is available from Fachinformationszentrum Karlsruhe, D-76344 Eggenstein-Leopoldshafen (Germany), by quoting the Registry No. CSD−421876.

Subsequent low-temperature data collections showed superstructure formation (puckering of the [$AuGe_3$] networks); however, the key to find the correct space group is hampered by non-space group specific extinctions, twinning, and satellite reflections. Detailed work on the low-temperature modification of Eu_2AuGe_3 is still going on and will be reported in a forthcoming paper.

Magnetic Measurements. Magnetic susceptibility measurements were carried out with a Quantum Design MPMS SQUID magnetometer. Single crystals of Eu_2AuGe_3 were loaded at random orientations into a gelatin capsule, mounted in a plastic straw and affixed to the end of a carbon fiber rod. Temperature dependent data were collected for both the zero field cooled (ZFC) and the field cooled mode (FC) between 2 and 300 K, with an applied field of 1 kG. Field dependent magnetic measurements were acquired at 5 K with field sweeping from −50 kG up to 50 kG. The raw data were corrected for the sample holder (straw) contribution.

Electrical Resistivity. The resistivity measurements were performed on a selected single crystal of around 1 mm in length and 500 μm thickness with a conventional AC four probe setup. Four very thin copper wires were glued to the pellet using a strongly conducting silver epoxy paste. The data were collected between 4.2 and 300 K using a PPMS. The results were reproducible for several crystals.

Specific Heat. Heat capacity (C_p) measurements were performed on selected single crystals of Eu_2AuGe_3, by a relaxation method using a QD-PPMS. The sample was glued to a calibrated HC-puck using Apiezon N grease. C was measured in the 3−50 K range without applied fields (H).

^{151}Eu Mössbauer Spectroscopy. The 21.53 keV transition of ^{151}Eu with an activity of 130 MBq (2% of the total activity of a ^{151}Sm:EuF_3 source) was used for the Mössbauer spectroscopic experiments, which were conducted in the usual transmission geometry. The measurements were performed with a commercial helium-bath cryostat. The temperature of the absorber was varied between 4.2 K and room temperature, while the source was kept at room temperature. The temperature was controlled by a resistance thermometer (±0.5 K accuracy). The sample was enclosed in a small PVC container at a thickness corresponding to about 10 mg Eu/cm^2.

Results and Discussion

Crystal Chemistry. Eu_2AuGe_3 crystallizes with a superstructure of the well-known AlB_2 family.[60] Within this family of superstructures, two main different coloring schemes of the honeycomb like networks are possible for ternary intermetallic compounds. The two simplest superstructures are presented in Figure 1. The 1:1 coloring on the hexagonal network leads to the SrPtSb[61] type structure,

(57) Yvon, K.; Jeitschko, W.; Parthé, E. *J. Appl. Crystallogr.* **1977**, *10*, 73–74.
(58) Cardoso Gil, R.; Carrillo-Cabrera, W.; Schultheiss, M.; Peters, K.; von Schnering, H. G.; Grin, Yu. *Z. Anorg. Allg. Chem.* **1999**, *625*, 285–293.
(59) Sheldrick, G. M. *SHELXL-97, Program for Crystal Structure Refinement*; University of Göttingen: Göttingen, Germany, 1997.
(60) Hoffmann, R.-D.; Pöttgen, R. *Z. Kristallogr.* **2001**, *216*, 127–145.
(61) Wenski, G.; Mewis, A. *Z. Anorg. Allg. Chem.* **1986**, *535*, 110–122.

Table 2. Refined Atomic Positions and Displacement Parameters of the Room-Temperature Modification of Eu_2AuGe_3, Space Group *Fmmm*

atom	Wyckoff pos.	*x*	*y*	*z*	U_{11}	U_{22}	U_{33}	U_{12}	U_{eq}[a]
Eu1	8*i*	0	0	0.24852(15)	93(7)	90(7)	64(6)	0	82(3)
Eu2	8*f*	1/4	1/4	1/4	86(7)	101(7)	70(6)	0	86(3)
Au	8*h*	0	0.66662(9)	0	69(6)	81(5)	139(5)	0	96(3)
Ge1	8*h*	0	0.1647(3)	0	63(15)	95(13)	399(17)	0	186(7)
Ge2	16*o*	0.2482(4)	0.08234(16)	0	64(10)	82(9)	354(12)	−3(8)	167(4)

[a] U_{eq} is defined as one-third of the derivative of the orthogonalized U_{ij}-tensor. The exponent of the anisotropic displacement parameters is defined through $\exp\{-2\pi^2(U_{11}h^2a^{*2} + ... + U_{12}hka^*b^*)\}$. $U_{13} = U_{23} = 0$.

Table 3. Interatomic Distances (pm) in the Room-Temperature Structure of Eu_2AuGe_3[a]

Eu1:	2	Ge1	331.5(4)	Au:	2	Ge2	249.6(3)
	4	Ge2	332.2(3)		1	Ge1	250.6(4)
	2	Au	335.4(2)		4	Eu2	334.6(1)
	4	Ge2	335.9(3)		2	Eu1	335.4(2)
	4	Eu2	428.8(2)	Ge1:	2	Ge2	245.5(4)
	2	Eu1	428.9(2)		1	Au	250.6(4)
	1	Eu1	447.4(3)		2	Eu1	331.5(4)
	1	Eu1	452.8(3)		4	Eu2	335.7(2)
Eu2:	4	Au	334.6(1)	Ge2:	1	Ge2	244.6(5)
	4	Ge1	335.7(2)		1	Ge1	245.5(4)
	4	Ge2	335.7(2)		1	Au	249.7(3)
	4	Eu1	428.8(2)		2	Eu1	332.2(3)
	2	Eu2	428.9(2)		2	Eu2	335.7(2)
	2	Eu2	450.1(2)		2	Eu1	335.9(3)

[a] All distances of the first coordination spheres are listed. Standard deviations are given in parentheses.

where the platinum and antimony atoms show trigonal planar coordination. Later on, several more complicated superstructures with differently tilted T_3X_3 hexagons have been observed.[60,62−69] With a higher *p* element content, ordered arrangements within the hexagonal networks are possible for compositions 2:1:3, and the simplest ordering variants are U_2RuSi_3 (Figure 1),[70] Ce_2CoSi_3,[71] and Eu_2PdSi_3.[72] Depending on the valence electron concentration and geometrical restraints, such compounds show different ordering patterns[73] and stacking sequences.[58,74−77]

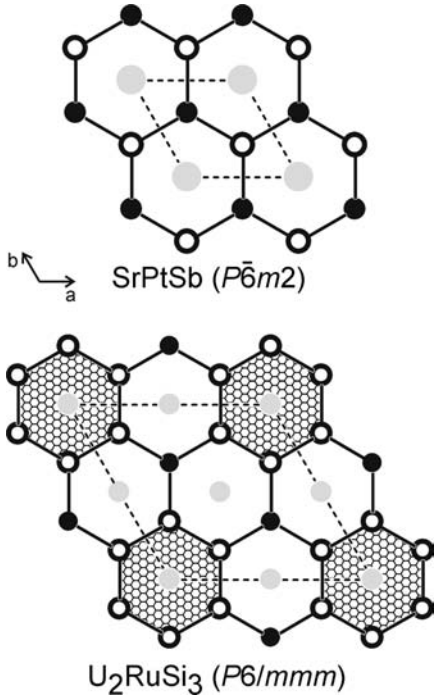

Figure 1. Coloring of honeycomb-like networks for compositions *TX* and TX_3, exemplarily shown for SrPtSb[61] and U_2RuSi_3.[70] Strontium (uranium), transition metal, and antimony (silicon) atoms are drawn as medium gray, black filled, and open circles, respectively. The [PtSb] and $[RuSi_3]$ networks are emphasized. The Hückel arene-like $[Si_6]^{10-}$ units in U_2RuSi_3 are shaded.

The germanide Eu_2AuGe_3 is isotypic with Ca_2AgSi_3[58] and shows the coloring pattern of the second type with slightly orthorhombically distorted Ge_6 and Au_2Ge_4 hexagons. A view of the Eu_2AuGe_3 structure approximately along the *a*-axis is presented in Figure 2. As is readily evident from this drawing, the substantial displacements of the two crystallographically independent germanium atoms off the mirror planes (i.e., along the *c*-axis) call for further symmetry reduction at low temperature. Preliminary investigations near liquid nitrogen temperature indeed show superstructure reflections which point to a modulated phase. The unit cell changes to $a = 854.25(18)$ pm, $b = 1789.7(3)$ pm, and $c = 854.25(17)$ pm and β changes to 119.98°. Detailed studies on the low-temperature structural behavior are in progress. At this point it is worthwhile to note that the Ca_2AgSi_3[58] type is a "stuffed" variant of the polyphosphide α-K_4P_6.[78] Recent solid state NMR data on the heavier analogues Rb_4P_6 and Cs_4P_6[79] showed non-aromaticity for the P_6^{4-} anions.

(62) Pöttgen, R.; Hoffmann, R.-D.; Müllmann, R.; Mosel, B. D.; Kotzyba, G. *Chem.—Eur. J.* **1997**, *3*, 1852–1859.
(63) Prots', Yu. M.; Pöttgen, R.; Jeitschko, W. *Z. Anorg. Allg. Chem.* **1998**, *624*, 425–432.
(64) Kussmann, D.; Hoffmann, R.-D.; Pöttgen, R. *Z. Anorg. Allg. Chem.* **1998**, *624*, 1727–1735.
(65) Prots', Yu. M.; Pöttgen, R.; Niepmann, D.; Wolff, M.; Jeitschko, W. *J. Solid State Chem.* **1999**, *142*, 400–408.
(66) Niepmann, D.; Prots', Yu. M.; Pöttgen, R.; Jeitschko, W. *J. Solid State Chem.* **2000**, *154*, 329–337.
(67) Hoffmann, R.-D.; Pöttgen, R.; Kussmann, D.; Müllmann, R.; Mosel, B. D. *Chem. Mater.* **2001**, *13*, 4019–4025.
(68) Hoffmann, R.-D.; Pöttgen, R.; Kussmann, D.; Niepmann, D.; Trill, H.; Mosel, B. D. *Solid State Sci.* **2002**, *4*, 481–487.
(69) Rodewald, U. Ch.; Heying, B.; Hoffmann, R.-D.; Niepmann, D.; Pöttgen, R. *Z. Naturforsch.* **2009**, *64b*, 595–602.
(70) Pöttgen, R.; Gravereau, P.; Darriet, B.; Chevalier, B.; Hickey, E.; Etourneau, J. *J. Mater. Chem.* **1994**, *4*, 463–467.
(71) Gordon, R. A.; Warren, C. J.; Alexander, M. G.; DiSalvo, F. J.; Pöttgen, R. *J. Alloys Compd.* **1997**, *248*, 24–32.
(72) Rodewald, U. Ch.; Hoffmann, R.-D.; Pöttgen, R.; Sampathkumaran, E. V. *Z. Naturforsch.* **2003**, *58b*, 971–974.
(73) Chevalier, B.; Pöttgen, R.; Darriet, B.; Gravereau, P.; Etourneau, J. *J. Alloys Compd.* **1996**, *233*, 150–160.
(74) Chevalier, B.; Lejay, P.; Etourneau, J.; Hagenmuller, P. *Solid State Commun.* **1984**, *49*, 753–760.
(75) Gladyshevskii, R. E.; Cenzual, K.; Parthé, E. *J. Alloys Compd.* **1992**, *189*, 221–228.
(76) von Schnering, H. G.; Bolle, U.; Curda, J.; Peters, K.; Carrillo-Cabrera, W.; Somer, M.; Schultheiss, M.; Wedig, U. *Angew. Chem.* **1996**, *108*, 1062–1064.
(77) Bolle, U.; Carrillo-Cabrera, W.; Peters, K.; von Schnering *Z. Kristallogr. NCS* **1998**, *213*, 689.
(78) Abicht, H. P.; Hönle, W.; von Schnering, H. G. *Z. Anorg. Allg. Chem.* **1984**, *519*, 7–23.
(79) Kraus, F.; Schmedt auf der Günne, J.; DiSalle, B. F.; Korber, N. *Chem. Commun.* **2006**, 218–219.

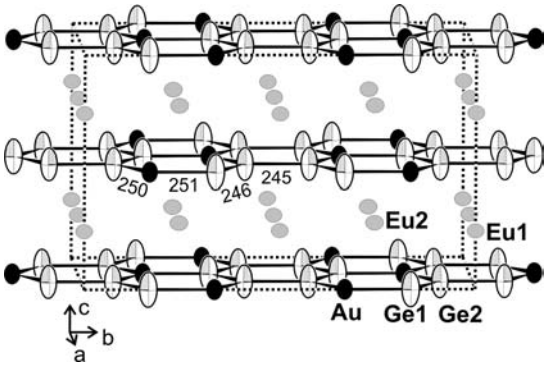

Figure 2. View of the Eu_2AuGe_3 structure approximately along the *a*-axis. Europium, gold, and germanium atoms are drawn as medium gray, black filled, and open circles, respectively. The two-dimensional [$AuGe_3$] networks, atom labels and relevant interatomic distances are highlighted.

Thus, one might expect also slightly distorted variants of the binaries at low temperature.

The shortest interatomic distances in the Eu_2AuGe_3 structure occur between the gold and germanium atoms (250−251 pm). They are slightly shorter than the sum of the covalent radii[80] of 256 pm. The Ge1−Ge2 (246 pm) and Ge2−Ge2 (245 pm) distances are similar to the diamond modification of germanium (245 pm).[81] We can thus assume strong covalent Au−Ge and Ge−Ge bonding within the two-dimensional [$AuGe_3$] networks. The Au−Ge distances in Eu_2AuGe_3 are remarkably short, when compared to 267−271 pm in EuAuGe[52] and 258−275 pm in ScAuGe[82] which are both also ordered AlB_2 superstructures, however, with strongly puckered Au_3Ge_3 hexagons.

Both europium sites have a slightly distorted hexagonal prismatic coordination, Eu1 with one Au_2Ge_4 and one Ge_6 and Eu2 with two Au_2Ge_4 hexagons. Because of the small distortions within the hexagons, we observe a narrow range for the Eu−Au (335) and Eu−Ge (332−336 pm) distances. The europium atoms have eight europium neighbors at Eu−Eu distances ranging from 429 to 453 pm. In view of the divalent nature of europium (vide infra) and the already shorter Eu−Eu distances of 397 pm in elemental *bcc* europium,[81] Eu−Eu bonding can safely be neglected in Eu_2AuGe_3.

Finally we turn back to the superstructure formation. The puckering of the T_3X_3 hexagons in the various AlB_2 superstructure variants depends on tiny external parameters, basically tiny differences in the radii of the constituents. To give an example, the equiatomic stannides CaAuSn,[64] SrAuSn,[68] EuAuSn,[62] and YbAuSn[67] all crystallize with pronounced KHg_2 type subcells; however, they built up different superstructures, a consequence of the difference in size between divalent Ca, Sr, Eu, and Yb. This driving force for superstructure formation will now be examined in detail also for the potential R_2AuGe_3 phases with strontium and ytterbium. Besides the difference in the radii, temperature also plays an important role as is indeed the case for Eu_2AuGe_3.

A further difference between the 1:1:1 and 2:1:3 AlB_2 superstructures concerns the interlayer bonding. Several

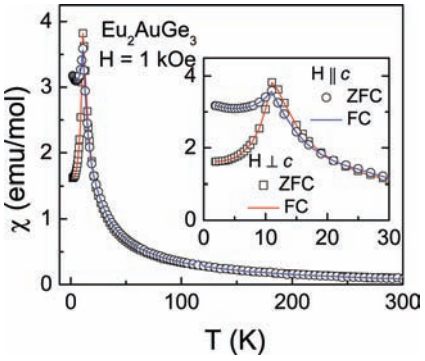

Figure 3. Magnetic susceptibility measured for a single crystal of Eu_2AuGe_3 in two different orientations, magnetic field along the *c*-axis (H ∥ *c*) and magnetic field perpendicular to the *c*-axis (H ⊥ *c*). The measurements were done in both zero field cooled (ZFC) and field cooled (FC) states of the crystal. The ZFC data are shown as open symbols, whereas the FC data is shown as continuous line. The inset shows the low temperature antiferromagnetic peak around 11 K seen in both orientations. The inset also highlights the magnetic anisotropy between the two orientations.

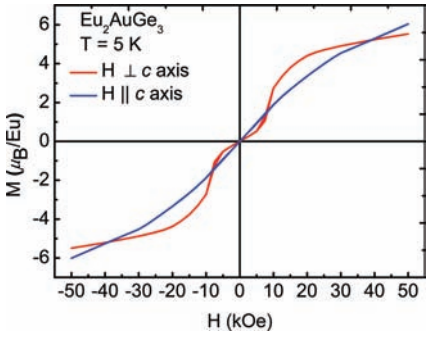

Figure 4. *M*(*H*) loops for a single crystal of Eu_2AuGe_3 measured with applied magnetic field perpendicular and parallel to *c* axis.

of the 1:1:1 gold containing compounds show a variety of Au−Au contacts. Such attractive d^{10}−d^{10} interactions are also a driving force for puckering of the T_3X_3 hexagons. Increasing the germanium content leads to a dilution of the transition metal content, and in the 2:1:3 known so far we observe no Au−Au contacts.

Magnetization. (a). Single Crystals. The magnetic susceptibility, χ, of a single crystal has been measured in two orientations, one being parallel to the applied magnetic field (marked as H ∥ *c*-axis) and other being perpendicular to the field (marked as H ⊥ *c*-axis). In both the measurements, χ increases gradually with increasing temperature and undergoes magnetic ordering (T_N) around 11 K. The χ falls rapidly above 11 K with increasing temperature up to 200 K and above 200 K decreases marginally.

The anisotropy between the perpendicular and the parallel directions of the single crystal is clearly evident from the inset of Figure 3. Below 11 K, it is seen that the behavior of $\chi(T)$ for both directions is slightly different in terms of the value of χ at the lowest temperature. For H ⊥ *c*, χ tends to saturate whereas for H ∥ *c* χ tends to increase as $T \rightarrow 0$.

Another evidence for the anisotropy between the two crystallographic orientations of Eu_2AuGe_3 can also be seen from the magnetization as a function of field in the magnetically ordered state, that is, $T < T_N$. Figure 4 shows the magnetization of the sample while varying the magnetic field with field applied parallel and perpendicular to the *c*-axis of the single crystal. Strong anisotropy effects

(80) Emsley, J. *The Elements*; Clarendon Press: Oxford, 1989.
(81) Donohue, J. *The Structures of the Elements*; Wiley: New York, 1974.
(82) Pöttgen, R.; Borrmann, H.; Felser, C.; Jepsen, O.; Henn, R.; Kremer, R. K.; Simon, A. *J. Alloys Compd.* **1996**, *235*, 170–175.

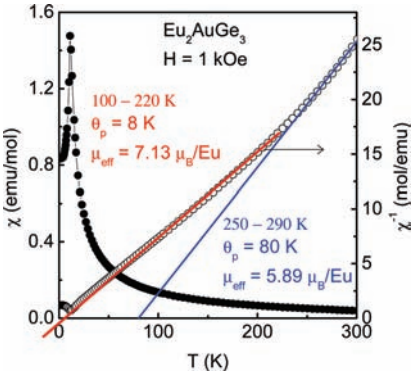

Figure 5. Magnetic susceptibility ($\chi = M/H$) as a function of temperature for a Eu_2AuGe_3 (polycrystalline) sample measured in a dc field of 1 kOe. Inverse magnetic susceptibility is also shown in the figure. The blue line passing through the data points is the fit to the Curie–Weiss law.

are observed in Eu_2AuGe_3. In the measurement done with magnetic field perpendicular to the *c*-axis ($H \perp c$), the system exhibits metamagnetism around 10 kOe, and tends to saturate at fields above 20 kOe. No hysteresis has been observed. For the $H \parallel c$ measurement, the moment increases nonlinearly with increasing field, with no trace of saturation until higher fields. Therefore one can attribute the magnetization of this compound to magnetic ions present on the basal plane.

(b). Bulk Sample in Powder Form. The molar magnetic susceptibility of a bulk sample of Eu_2AuGe_3 measured in a field of 1 kOe, (Figure 5), also exhibits a sharp peak around 11 K indicating transition to the antiferromagnetic state in agreement with the single crystal measurement. Qualitatively, the data of the bulk sample is similar to data measured on a single crystal with field perpendicular to the *c*-axis. Below 11 K, in the magnetically ordered state, the system exhibits complex magnetism. Above T_N, the $\chi(T)$ falls rather sharply and decreases with increasing temperature.

The plot of inverse susceptibility (χ^{-1}) as a function of temperature deviates from linearity (the Curie–Weiss behavior) below 200 K. Though there is no abrupt anomaly, there is a definite change in slope around this temperature. The fit to the Curie–Weiss law in the temperature range of 250–300 K, gives the value of paramagnetic Curie temperature (θ_p) of 80 K and an effective Bohr magneton number (μ_{eff}) of 5.89 μ_B/Eu ions. As discussed above, the title compound undergoes a structural transition around 130 K, the deviation of $\chi^{-1}(T)$ below 200 K can be taken as an indication of this transition. As there is no corresponding anomaly in $\chi(T)$, the structural transition can be of the second order. The fit to the Curie–Weiss law in the temperature range of 100–220 K, gives the value of the paramagnetic Curie temperature (θ_p) of 7.5 K and an effective Bohr magneton number (μ_{eff}) of 7.13 μ_B/Eu ion. The value of μ_{eff} is slightly lower than the expected free ion moment of $Eu^{2+} = 7.94\ \mu_B$, and can be attributed to factors such as crystal field effects.

Specific Heat Data. The specific heat of Eu_2AuGe_3 is shown in Figure 6. The data clearly exhibit a Λ-shaped peak at 11 K, exhibiting long-range antiferromagnetic ordering in the system. However, the peak close to 24 K raises an interesting question regarding the origin of such a distinctive Λ-like peak at this temperature. The events responsible for these two peaks in the specific heat are corroborated by corresponding resistivity data presented

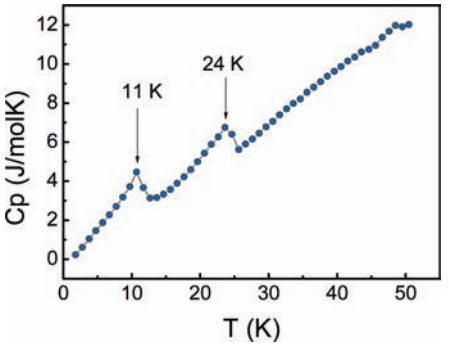

Figure 6. Heat capacity (C_p) for Eu_2AuGe_3 measured as a function of temperature (T) at zero applied fields.

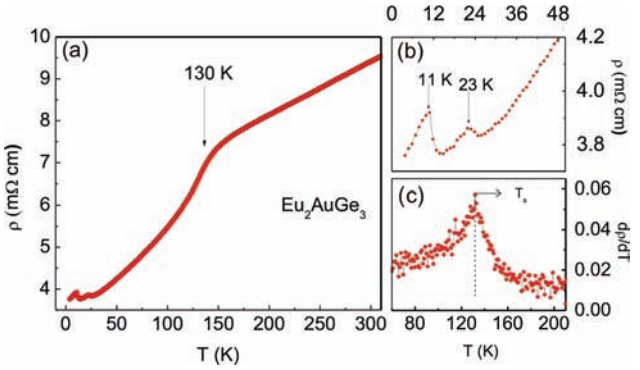

Figure 7. (a) Temperature dependence of the electrical resistivity of Eu_2AuGe_3 with zero applied magnetic field. The arrow shown at 130 K is the structural transformation. (b) Low temperature resistivity data on an expanded scale showing the peaks at 11 and 23 K which correspond to antiferromagnetic ordering and possible ferromagnetic cluster formation, respectively. (c) First derivative of $\rho(T)$. The dotted line exhibits the temperature of structural transition.

below. A close inspection of $\chi(T)$ (Figure 3) shows that χ rises sharply below 25 K, reminiscent of a ferromagnetic like ordering. This is further evidenced by the positive θ_p values, which indicates ferromagnetic correlations. Therefore, considering the specific heat measurements, the peak at ~24 K could be due to ferromagnetic cluster formation. On further cooling, the system undergoes antiferromagnetic ordering ~11 K; however, as the system is not completely in the antiferromagnetic state, the moment values do not fall to zero as $T \rightarrow 0$.

Within the Debye theory, the low temperature approximation of the measured specific heat is given as $C_p = \gamma T + \beta T^3$ or $C_p/T = \gamma + \beta T^2$ where γ is the contribution from the conduction electrons and β is the lattice contribution.[83] We have fitted the linear region of the C_p/T versus T plot ($T < 11$ K), and observed that the electronic and lattice contributions are 300 mJ/mol K^2 and 1 mJ/mol K^4, respectively.

Electrical Resistivity. The temperature dependence of the resistivity of single crystal samples of Eu_2AuGe_3 is plotted in Figure 7a. The resistivity decreases with decreasing temperature which is typical for a metallic conductor. The data also confirms two magnetic orderings in this compound. Figure 7b exhibits $\rho(T)$ on an expanded scale, which shows the peaks at 11 and 23 K respectively in good

(83) Gopal, E. S. R. *Specific heat at low temperatures*; Plenum: New York, 1966.

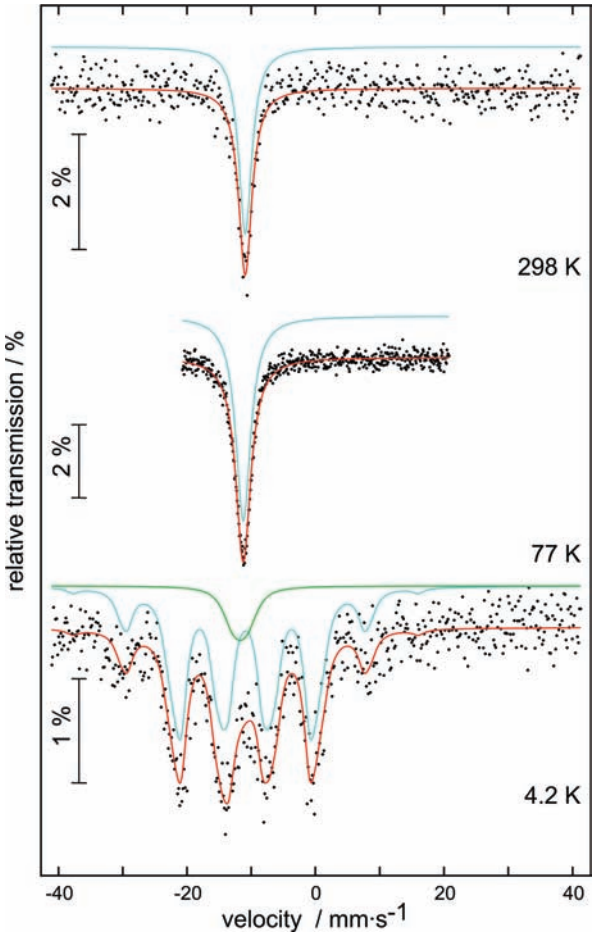

Figure 8. Experimental and simulated ^{151}Eu Mössbauer spectra of Eu_2AuGe_3 at various temperatures.

agreement with the magnetic and heat capacity data. The linear dependence of the resistivity of Eu_2AuGe_3 at temperatures below and above 130 K can be attributed to electron−phonon scattering. This is more clearly seen in the plot of $d\rho/dT$ shown in Figure 7c. In the systems undergoing second order structural transitions, the effect of spin-fluctuations in the paramagnetic region becomes important, and this can be clearly seen as a peak in the plot of $d\rho/dT$ versus T.[84,85] Therefore, the anomaly around 130 K in the plot of $\rho(T)$ can be attributed to the change in the crystal structure.

^{151}Eu Mössbauer Spectroscopy. The ^{151}Eu Mössbauer spectra of the Eu_2AuGe_3 sample at 298, 77, and 4.2 K are presented in Figure 8 together with transmission integral fits. The corresponding fitting parameters are summarized in Table 4. At 298 and 77 K, well above the magnetic ordering temperature the spectra could be fitted with a single signal at an isomer shift close to 11 mm/s, indicative for purely divalent europium, in agreement with the susceptibility measurements. The experimental line width is slightly increased with respect to the typical value of ~2.3 mm/s observed for intermetallic compounds. This can be attributed to the two crystallographically independent europium sites which show superposition in the experimental spectrum.

Table 4. Fitting Parameters of ^{151}Eu Mössbauer Spectroscopic Measurements of Eu_2AuGe_3[a]

T/K	δ/mm·s^{-1}	Γ/mm·s^{-1}	ΔE_Q/mm·s^{-1}	B_{Hf}/T	ratio
298	−10.93(4)	2.50(9)	0.0*		
77	−11.24(1)	2.82(3)	0.0*		
4.2	−10.88(4)	2.27(11)	0.0*	26.0(1)	89%
4.2	−11.7(1)	2.8*	0.0*	3.5(8)	11%

[a] Numbers in parentheses represent the statistical errors in the last digit. (δ), isomer shift; (Γ), experimental line width: (ΔE_Q) electric quadrupole splitting; (B_{Hf}) magnetic hyperfine field. Numbers marked with an asterisk were fixed during the fitting procedure.

At 4.2 K, in the magnetically ordered regime we observe magnetic hyperfine field splitting. The spectrum could be well reproduced by a superposition of two spectral components. The main component with 89% contribution at $\delta = -10.88(4)$ mm/s shows a magnetic hyperfine field of 26.0(1) T, typically observed for europium intermetallics.[86] This signal is superimposed by a second contribution with 11% intensity at $\delta = -11.7(1)$ mm/s and a small hyperfine field of only 3.5(8) T. This behavior can be explained with a domain structure within our sample. The major part of the sample shows full magnetic order, while a small degree of the domains shows no magnetic long-range ordering. This can be due to small deviations from the ideal compositions, that is, domains $Eu_2Au_{1\pm x}Ge_{3\pm x}$. This is likely to occur in such a complex superstructure with eight crystallographically independent europium sites. This may also explain the clustering behavior discussed above.

The isomer shift in Eu_2AuGe_3 at 77 K (−11.24 mm/s) is slightly smaller than in equiatomic EuAuGe (−10.30 mm/s).[52] This is in agreement with a slightly higher ionicity (smaller s electron density) in Eu_2AuGe_3.

Concluding Remarks

Eu_2AuGe_3 is an AlB_2 structure variant which shows temperature dependent polymorphism. The room temperature structure (Ca_2AgSi_3 type) was refined from single crystal diffractometer data. Magnetic susceptibility and ^{151}Eu Mössbauer spectroscopic data show exclusively divalent europium. Eu_2AuGe_3 orders antiferromagnetically at 11 K and shows a metamagnetic transition at 10 kOe. The compound undergoes a structure change below 130 K as determined by X-ray diffraction and supported by resistivity and magnetic susceptibility measurements. Understanding the reasons for the phase transitions will require theoretical electronic structure calculations and the study of nonmagnetic isostructural analogues such as Ca_2AuGe_3. Our experimental work indicates that the isostructural compounds Ca_2AuGe_3 and Sr_2AuGe_3 are also stable.

Acknowledgment. Financial support from the Department of Energy (Grant DE-FG02-07ER46356) and the Deutsche Forschungsgemeinschaft are gratefully acknowledged. Use was made of facilities operated by the Northwestern Materials Research Center under NSF Grand DMR-0520513. Technical support was provided by Dr. O. Chernyashevskyy.

Supporting Information Available: Crystallographic data in CIF format. This material is available free of charge via the Internet at http://pubs.acs.org.

(84) Pereira, A. M.; Magen, C.; Braga, M. E.; Pinto, R. P.; Fermento, R.; Algarabel, P. A.; Morellon, L.; Ibarra, M. R.; Araujo, J. P.; Sousa, J. B. *J. Non-Cryst. Solids* **2008**, *354*, 5298.
(85) Pecharsky, V. K.; Gschneidner, K. A. *Adv. Mater.* **2001**, *13*, 683.
(86) Pöttgen, R.; Johrendt, D. *Chem. Mater.* **2000**, *12*, 875–897.